

Cantilevered, Rectangular Plate Dynamics by Finite Difference Methods

Benjamin Brown
University of Maryland, Baltimore County
Baltimore, MD
bbrown4@umbc.edu

October 8, 2021

Abstract

In this technical note, we consider a dynamic linear, cantilevered rectangular plate. The evolutionary PDE model is given by the fourth order plate dynamics (via the spatial biharmonic operator) with clamped-free-free-free boundary conditions. We additionally consider damping/dissipation terms, as well as non-conservative lower order terms arising in various applications. Dynamical numerical simulations are achieved by way of a finite difference spatial approximation with a MATLAB time integrator. The rectangular geometry allows the use of standard 2D spatial finite differences, while the high spatial order of the problem and mixed clamped-free type boundary conditions present challenges. Dynamic energies are also computed. The relevant code is presented, with discussion of the model and context.

1 Introduction

The purpose of this note is to describe a dynamic simulation method for a linear 2D cantilevered plate via finite differences. We specifically determine the ghost points required for the enforcement of the cantilever boundary conditions (mixed clamped-free with corners).

1.1 Motivation

The primary motivation for studying the particular PDE model below derives from the application of piezoelectric energy harvesting [14, 13]. In this application, a cantilevered beam or rectangular plate is placed in a surrounding flow of air. In the *axial* configuration (whereby the flow runs from clamped end to free end of the structure), a cantilever is particularly prone to an aeroelastic instability termed *flutter*, even for low flow speeds. After the onset of instability, the beam settles into a limit cycle oscillation. If a piezo-electric device (for instance a thin layer, or patch) is affixed to the deflecting structure, power is generated and can be harvested. The energy is produced by the system's sustained large, flapping motion which causes a current to be produced via the piezoelectric effect. Such energy-harvesting configurations have recently been shown to be viable [14]. As an alternative energy source, scaled harvester systems could be effective in providing power to remote locations, or small surges of power to supplement a traditional grid.

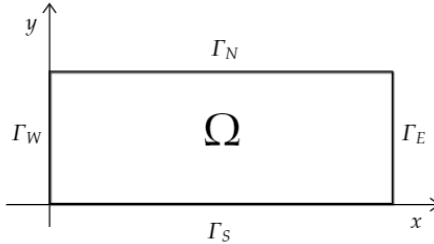
To effectively and efficiently harvest energy from the flow-induced oscillations of an elastic cantilever, one must have a viable distributed parameter system describing the large deflections of the 1D or 2D cantilevered structure. In particular, to produce a limit cycle oscillation in the post-flutter regime (i.e., after the onset of the flow-induced bifurcation), the structural model must permit large deflections and incorporate a nonlinear restoring force. Recent work has 1D

inextensible cantilevers, including modeling [8, 7], and more recently, a well-posedness analysis of solutions [5]. More recently, the modeling work was extended to (several) 2D inextensible cantilevered plates [6]. These plate models are very involved, including nonlinear inertial and stiffness terms, as well as Lagrange multipliers for the enforcement of relevant constraints. In this note, we focus on the linearization of the model in [6], and provide a fast numerical solver for a plate with given forcing (through the boundary and the right hand side). We accommodate damping effects, and crude approximations of the flow via a linear piston-theoretic approximation of potential flow (see, e.g., [10]). This model is can be used viably in the pre-onset regime, as well as to compute a flow-induced bifurcation point via the non-conservative flow parameters. Additionally, the code is general enough to compute dynamic responses to arbitrary edge loading, as well as dynamic and spatially distributed right hand sides.

Much numerical work has been done on linear cantilevered models in 1D [11, 10, 7], however much less mathematical literature exists for 2D cantilevered plate models, likely owing to the challenges associated to the high order of the problem and requisitely mixed (with corners) boundary conditions¹. We call attention to one older technical note that discusses finite difference stencils for rectangular plates with different boundary conditions [2]—the analysis there is entirely static. It is clear, in general, that 2D models (and associated simulations), are necessary for the engineering applications mentioned above. We resolve the PDE dynamics below using finite difference methods with careful calculations of ghost nodes that allow algebraic corner conditions to be properly solved.

1.2 Setup and Model

An open rectangular domain, Ω with boundary $\Gamma = \overline{\Gamma_E} \cup \overline{\Gamma_N} \cup \overline{\Gamma_W} \cup \overline{\Gamma_S}$, will be used for this model, and will use cardinal coordinates for naming, as can be seen in the following diagram:



The linear cantilevered plate model, with the rectangular domain Ω , is described by the following equations:

$$\begin{cases} w_{tt} + D\Delta^2 w + k_0 w_t - k_1 \Delta w_t + a_1 w_x + a_2 w_y = f(x, t) & \text{in } \Omega \\ w = \frac{\partial w}{\partial n} = 0 & \text{on } \Gamma_W \\ \nu w_{xx} + w_{yy} = g_1(x, y), \quad w_{yyy} + (2 - \nu)w_{xxy} = h_1(x, y) & \text{on } \Gamma_N \\ \nu w_{xx} + w_{yy} = g_2(x, y), \quad w_{yyy} + (2 - \nu)w_{xxy} = h_2(x, y) & \text{on } \Gamma_S \\ w_{xx} + \nu w_{yy} = g_3(x, y), \quad w_{xxx} + (2 - \nu)w_{yyx} = h_3(x, y) & \text{on } \Gamma_E \\ w(t = 0) = w_0(x), \quad w_t(t = 0) = w_1(x) & \end{cases} \quad (1)$$

The quantity $\nu \in (0, 1/2)$ represents the Poisson ratio [6]. Above, the function $w : \overline{\Omega} \times [0, T) \rightarrow \mathbf{R}$ represents the transverse displacement of a thin, isotropic, homogeneous plate. We do not explicitly incorporate piezoelectric effects here, and, assuming a piezoelectric material is attached to the surface of the plate, we incorporate the combined the combined stiffness effect through the

¹The mixed nature of the boundary conditions, as well as the corner angles, are known to affect the expected solution regularity—and also numerical convergence—near corners [3].

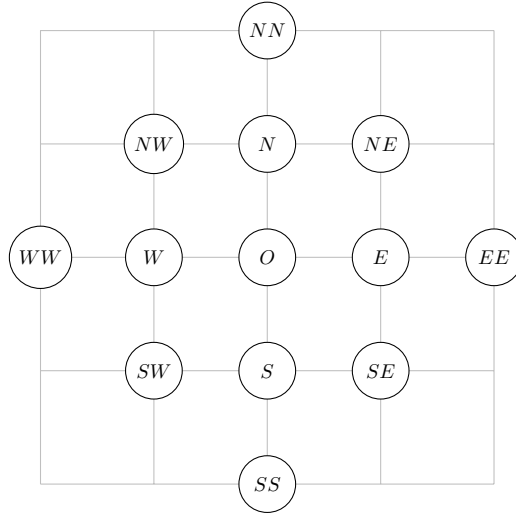


Figure 1: The 13-point stencil used in the finite difference method to approximate a fourth derivative

parameter $D > 0$. The damping coefficients are $k_0, k_1 \geq 0$, where the former measures weak or frictional damping, and the latter is so-called *square-root type damping* and is of a stronger nature. (See the discussion in [11] for further discussion about the interpretation and physical meaning of this type of damping.) In reality, the term $-k_1 \Delta w_t$ term may have questionable meaning for the cantilever, but is left in the implementation as it is unproblematic mathematically; we set $k_1 = 0$ for all examples shown throughout this note. The flow-velocity parameters are a_1, a_2 corresponding to the respective x and y components of the surrounding airflow. A linear combination of these, for instance, represents an off-axis flow; pure axial flow would take $a_1 > 0$ and $a_2 = 0$. The functions $g_i(x, y)$ correspond to edge-loading by way of boundary moments, while the boundary shears are given by $h_i(x, y)$ on each of the non-clamped boundaries in the model. The function $f(x, t)$ provides a distributed loading across the surface of Ω . In practice, for regular solutions, these boundary and interior data must satisfy natural compatibility conditions, in particular at/near corner points.

Due to the fourth order bi-harmonic operator, each point in the mesh created on the plate must be capable of having a 13-point stencil applied, including the edges and corners, such as in Figure 1. Owing to this, ghost points must be added around the boundary of the plate. To wit, a *ghost point* or *ghost node* is an artificial value for a point that created outside of $\bar{\Omega}$ to enforce the boundary conditions, permitting a finite difference stencil to be applied when the stencil overlaps boundary nodes. The particular challenges in the resolution and regularity of a given solution at corner points manifests themselves in algebraic issues for finite difference methods. Ghost points are calculated through using the boundary conditions, as well as known values from the interior, both of which are obtained through the data in the problem (e.g., f , g_i , and/or h_i). Indeed, the ghost node calculations are a central contribution of this note.

2 Ghost Points

As alluded to above, the inherent mixed boundary conditions in the cantilever problem introduce complications into the calculation of the ghost points. To determine ghost node values, we will begin with the clamped edge, because it is simple and only has one unknown. This will provide information to supply to more stencils in latter calculations of nodal values.

The nomenclature used in this section makes use of *cardinal values* that correspond to the current displacement of the point in the stated direction, with O representing the ‘origin’. For example, E refers to the mesh point to the right of O .

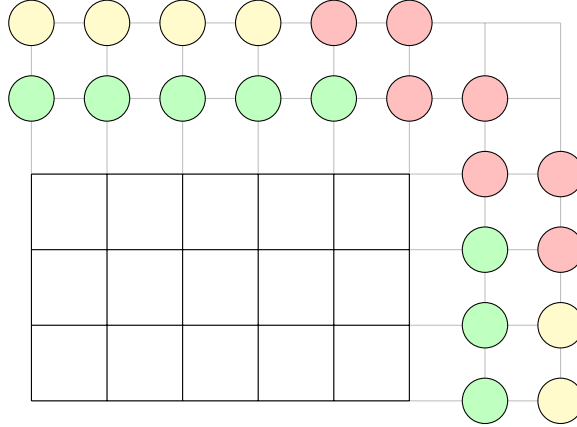


Figure 2: Diagram showing the order of ghost points being calculated around a free-free corner. Begin by calculating the first row, which are the green nodes. Then the second row will be calculated, represented by yellow nodes. Finally the system of seven equations can be solved for the corner nodes, shown in red.

2.1 Clamped Edge

On this edge, the conditions require that $w = 0$ and $w_x = 0$. Using the finite difference approximation on this point:

$$E = W,$$

for all O along the clamped boundary.

2.2 Free Edge

All of the following calculations will be made for the Γ_N boundary, but they apply to the other edges with a simple rotation of coordinates as needed.

The conditions on the three free edges require specified moments and shears:

$$\begin{cases} \nu w_{xx} + w_{yy} = g_1(x, y), & w_{yyy} + (2 - \nu)w_{xxy} = h_1(x, y) & \text{on } \Gamma_N \\ \nu w_{xx} + w_{yy} = g_2(x, y), & w_{yyy} + (2 - \nu)w_{xxy} = h_2(x, y) & \text{on } \Gamma_S \\ w_{xx} + \nu w_{yy} = g_3(x, y), & w_{xxx} + (2 - \nu)w_{yyx} = h_3(x, y) & \text{on } \Gamma_E \end{cases}$$

Because a 13-point stencil will be needed for the final calculation, two rows of ghost points must be determined.

2.2.1 First Row on Edge: Avoiding Corners

The second order boundary condition will be used for the first row. The free-free corner will be avoided for this calculation, as it has special calculations, shown later. Using the finite difference method to approximate this condition yields the following expression:

$$\frac{\nu (W - 2O + E)}{dx^2} + \frac{N - 2O + S}{dy^2} = g_1(x, y).$$

Notice that along all the free edges, except when adjacent to a free-free corner, there is only one unknown value, the ghost value. This can be explicitly solved for, for example on the southern edge, to give the requisite value of the ghost point:

$$S = -\frac{\nu (W - 2O + E) dy^2}{dx^2} - N + 2O + g_1(x, y).$$

2.2.2 Second Row on Edge: Avoiding Corners

The second boundary condition will be used for the second row of ghost points. When this stencil is utilized, and the first edge has already been calculated, the second row ghost values can then be solved directly. This calculations uses ghost nodes found in the previous step in the first row. Because of this, there must again be caution about the corner. The nodes to be calculated are shown in Figure 2 as the yellow nodes. Using the finite difference approximation on the second boundary condition yields the following expression:

$$\frac{SS - 2S + 2N - NN}{2 dy^3} + \frac{(2 - \nu)(SE - NE - 2S + 2N + SW - NW)}{2 dx^2 dy} = h_1(x, y).$$

The ghost point SS can be determined from the above, as it is the only unknown when applied to the southern free edge. The expression for this value is:

$$SS = -\frac{(2 - \nu) dy^2 (SE - NE - 2S + 2N + SW - NW)}{dx^2} + 2S - 2N + NN + h_1(x, y).$$

2.2.3 Corners

For each of the two free-free corners, there are seven unknown ghost points. We can make a linear system of the seven boundary conditions that can be applied to the surrounding points in order to explicitly find each of them. In this section, **for simplicity, the $g_i(x, y)$ and $h_i(x, y)$ terms will be set to zero.** In a latter section we will elaborate upon the edge loading conditions.

The relevant finite difference boundary conditions are:

$$\left\{ \begin{array}{l} \frac{\nu(W - 2O + E)}{dx^2} + \frac{N - 2O + S}{dy^2} = 0 \\ \frac{W - 2O + E}{dx^2} + \frac{\nu(N - 2O + S)}{dy^2} = 0 \\ \frac{SS - 2S + 2N - NN}{2 dy^3} + \frac{(2 - \nu)(SE - NE - 2S + 2N + SW - NW)}{2 dx^2 dy} = 0 \\ \frac{SSW - 2SW + 2NW - NNW}{2 dy^3} + \frac{(2 - \nu)(S - N - 2SW + 2NW + SWW - NWW)}{2 dx^2 dy} = 0 \\ \frac{EE - 2E + 2W - WW}{2 dx^3} + \frac{(2 - \nu)(SE - SW - 2E + 2W + NE - NW)}{2 dy^2 dx} = 0 \\ \frac{SEE - 2SE + 2SW - SSW}{2 dx^3} + \frac{(2 - \nu)(SSE - SSW - 2SE + 2SW + E - W)}{2 dy^2 dx} = 0 \\ SE - NE - SW + NW = 0 \end{array} \right.$$

Solving this system of boundary conditions yields the expressions for each ghost point about corner O , when O is the corner between Γ_N and Γ_E :

$$\left\{ \begin{array}{l} E = 2O - W \\ N = 2O - S \\ NE = SE - SW + NW \\ EE = \frac{(-4O + 4W + 2SE - 2SW)(\nu - 2)dx^2}{dy^2} + (4O - 4W + WW) \\ NN = \frac{(-4O + 4S + 2NW - 2SW)(\nu - 2)dy^2}{dx^2} + (4O - 4S + SS) \\ NNW = \frac{(\nu - 2)(2O - SSW - 2S - 2NW + 2SW + NWW)dy^2}{dx^2} + (2NW - 2SW + SSW) \\ SEE = \frac{(\nu - 2)(2O - W - 2SE + 2SW + 2SSE - SSW)dy^2}{dx^2} + (2SWW + 2SE - 2SW) \end{array} \right.$$

The same approach can be applied to the Γ_S and Γ_E corner, and the results are simply a reflection of these expressions.

3 Non-zero Edge Conditions

In the previous section the $g_i(x, y)$ and $h_i(x, y)$ values were set to be zero. This was done for simplicity, and clarity of exposition; in this section we provide examples of ghost node calculations with constant edge loading. As in the theory of boundary lifts, we can compute the solution from a given edge loading, while setting all other boundary loads to zero. The response to several edge loads can thus be reconstructed for the linear problem through the principle of superposition.

In this section, a derivation of nonzero, constant values will be shown, and the result of these loads will be determined. Again we shall only solve for the Γ_N boundary, but other boundary values will be determined via rotation.

We first handle the case where $g_i(x, y) = G$ and $h_i(x, y) = 0$. The conditions for this case become:

$$\left\{ \begin{array}{l} \frac{\nu(W-2O+E)}{dx^2} + \frac{N-2O+S}{dy^2} = G \\ \frac{W-2O+E}{dx^2} + \frac{\nu(N-2O+S)}{dy^2} = G \\ \frac{SS-2S+2N-NN}{2dy^3} + \frac{(2-\nu)(SE-NE-2S+2N+SW-NW)}{2dx^2dy} = 0 \\ \frac{SSW-2SW+2NW-NNW}{2dy^3} + \frac{(2-\nu)(S-N-2SW+2NW+SWW-NWW)}{2dx^2dy} = 0 \\ \frac{EE-2E+2W-WW}{2dx^3} + \frac{(2-\nu)(SE-SW-2E+2W+NE-NW)}{2dy^2dx} = 0 \\ \frac{SEE-2SE+2SW-SWW}{2dx^3} + \frac{(2-\nu)(SSE-SSW-2SE+2SW+E-W)}{2dy^2dx} = 0 \\ SE - NE - SW + NW = 0 \end{array} \right.$$

Solving this system for the conditions, as done previously, provides the solution:

$$\left\{ \begin{array}{l} E = 2O - W + \frac{Gdx^2}{\nu+1} \\ N = 2O - S + \frac{Gdy^2}{\nu+1} \\ NE = SE - SW + NW \\ EE = \frac{(-4O+4W+2SE-2SW)(\nu-2)dx^2}{dy^2} + (4O - 4W + WW) - \frac{2Gdx^4\nu-4Gdx^4}{dy^2(\nu+1)} + \frac{2Gdx^2}{\nu+1} \\ NN = \frac{(-4O+4S+2NW-2SW)(\nu-2)dy^2}{dx^2} + (4O - 4S + SS) - \frac{2Gdy^4\nu-4Gdy^4}{dx^2(\nu+1)} + \frac{2Gdy^2}{\nu+1} \\ NNW = \frac{(\nu-2)(2O-SW-2SW+2SW+2NW+2NW)dy^2}{dx^2} + (2NW - 2SW + SSW) + \frac{G(-2+\nu)dy^4}{dx^2(\nu+1)} \\ SEE = \frac{(\nu-2)(2O-W-2SE+2SW+2SSE-SSW)dy^2}{dx^2} + (2SWW + 2SE - 2SW) + \frac{G(-2+\nu)dx^4}{dy^2(\nu+1)} \end{array} \right.$$

Similarly we can consider the case where $g_i(x, y) = 0$ and $h_i(x, y) = H$. The conditions for this system become:

$$\left\{ \begin{array}{l} \frac{\nu(W-2O+E)}{dx^2} + \frac{N-2O+S}{dy^2} = 0 \\ \frac{W-2O+E}{dx^2} + \frac{\nu(N-2O+S)}{dy^2} = 0 \\ \frac{SS-2S+2N-NN}{2dy^3} + \frac{(2-\nu)(SE-NE-2S+2N+SW-NW)}{2dx^2dy} = H \\ \frac{SSW-2SW+2NW-NNW}{2dy^3} + \frac{(2-\nu)(S-N-2SW+2NW+SWW-NWW)}{2dx^2dy} = H \\ \frac{EE-2E+2W-WW}{2dx^3} + \frac{(2-\nu)(SE-SW-2E+2W+NE-NW)}{2dy^2dx} = H \\ \frac{SEE-2SE+2SW-SWW}{2dx^3} + \frac{(2-\nu)(SSE-SSW-2SE+2SW+E-W)}{2dy^2dx} = H \\ SE - NE - SW + NW = 0 \end{array} \right.$$

The solutions for this system are:

$$\left\{ \begin{array}{l} E = 2O - W \\ N = 2O - S \\ NE = SE - SW + NW \\ EE = \frac{(-4O+4W+2SE-2SW)(\nu-2)dx^2}{dy^2} + (4O - 4W + WW) + 2Hdx^3 \\ NN = \frac{(-4O+4S+2NW-2SW)(\nu-2)dy^2}{dx^2} + (4O - 4S + SS) - 2Hdx^3 \\ NNW = \frac{(\nu-2)(2O-SWW-2S-2NW+2SW+2NW)dy^2}{dx^2} + (2NW - 2SW + SSW) - 2Hdx^3 \\ SEE = \frac{(\nu-2)(2O-W-2SE+2SW+2SSE-SSW)dy^2}{dx^2} + (2SWW + 2SE - 2SW) + 2Hdx^3 \end{array} \right.$$

4 Reduction of Order and ODE Solver

To integrate in time, and produce distributed values at each time step, we invoke MATLAB's `ode15s` solver. This solver requires an abstract differential equation of the form:

$$\dot{y} = F(t, y). \quad (2)$$

To reduce our evolutionary PDE, we introduce states to reduce the order and create a 2×2 system in the state variables to obtain a first order formulation. The problem also has many spatial nodes, which each must be resolved. A matrix expression will be used to obtain one principal variable y to feed to the solver. We begin with the interior PDE:

$$w_{tt} + D\Delta^2 w + a_1 w_x + a_2 w_y + k_0 w_t - k_1 (w_{txx} + w_{tyy}) = f(x, t), \quad (3)$$

and introduce the state variable v , capturing w_t , or the velocity. We can also take the derivative of v and using the PDE expression for w_{tt} , we obtain the value of v_t :

$$\begin{cases} v = w_t \\ v_t = f(x, t) - D\Delta^2 w - a_1 w_x - a_2 w_y - k_0 w_t + k_1 (w_{txx} + w_{tyy}). \end{cases} \quad (4)$$

We can write each of these as a matrix:

$$y = \begin{bmatrix} w \\ v \end{bmatrix}, y_t = \begin{bmatrix} w_t \\ v_t \end{bmatrix}$$

For each node in the model we must solve for w and v , and thus we will extend each of these in the array with indices corresponding to each point in the mesh. There are a total of N nodes, determined from user set parameters as laid out in Section 6.

$$y = [w_1, w_2, \dots, w_N, v_1, v_2, \dots, v_N]^T$$

Using these vectors, this problem is now written as a first order ODE, and can be solved directly with the `ode15s` solver, where each iteration will be stored for future animation, post-processing calculations, and other data analyses. Appendix A contains MATLAB code used to simulate the plate dynamics.

5 Energy Calculation

The natural potential energy associated to a free plate is expressed in terms of the bilinear form

$$a(u, v) = \nu(\Delta u, \Delta v) + (1 - \nu)[(u_{xx}, v_{xx}) + 2(u_{xy}, v_{xy}) + (u_{yy}, v_{yy})], \quad (5)$$

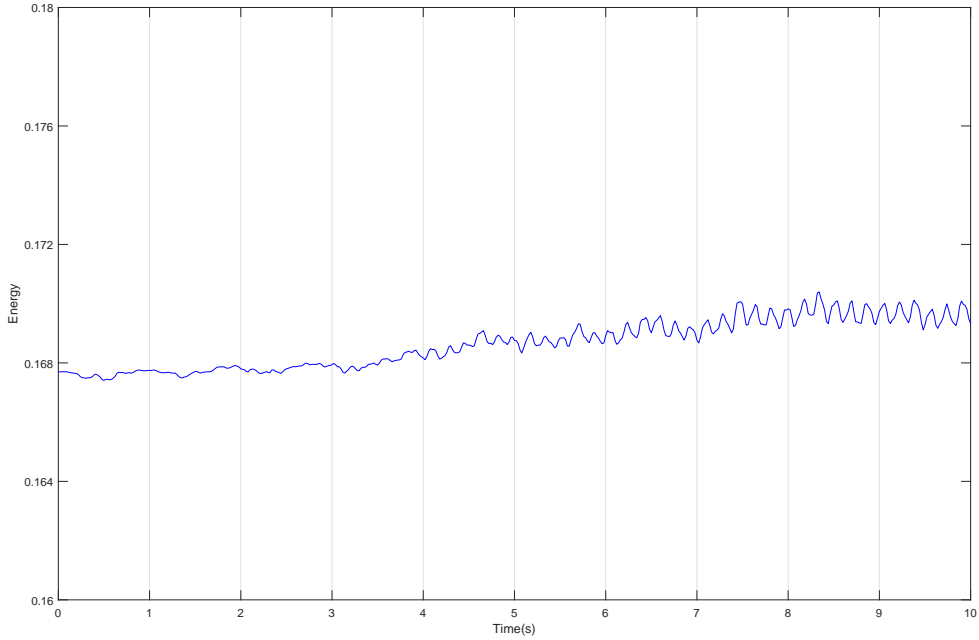


Figure 3: Conservation of energy demonstrated with a 10x10 mesh grid and $k_0 = k_1 = a_1 = a_2 = 0$, $v(x, y; 0) = x$

where the expression (f, g) represents the $L^2(\Omega)$ inner-product:

$$(f, g) = (f, g)_{L^2(\Omega)} = \int_{\Omega} f(x, y)g(x, y)d\mathbf{x}.$$

We consider the standard kinetic and potential contributions to the total energy. This is to say, for a state $[w, v]$ we can compute the total energy as

$$E(t) = E(w(t), v(t)) = U(w(t)) + K(v(t)).$$

The potential energy is given through the bilinear form as $U(w) = a(w, w)$:

$$U(w(t)) = \frac{1}{2}D \int_{\Omega} [\nu(\Delta w(t))^2 + (1 - \nu)(w_{xx}^2(t) + 2w(t)_{xy}^2 + w(t)_{yy}^2)] d\mathbf{x}$$

and the kinetic energy

$$K(v) = \frac{1}{2} \int_{\Omega} v(t)^2 d\mathbf{x},$$

where we have suppressed the dependence of the states on \mathbf{x} .

If there is no damping or flow considered in the model (i.e., $k_0 = k_1 = a_1 = a_2 = 0$), then conservation of energy is expected for solutions—see, for instance, [5, 10]. We demonstrate this here with an initial state consisting of an initial displacement of $w(x, y; 0) = 0$ and an initial velocity of $v(x, y; 0) = x$. Figure 3 is produced by the script and demonstrates the conservation of energy for the numerically computed solution in this situation.

Of course, slight variations (errors) can be observed on this small scale due to numerical error in the finite difference method and time integrator used.

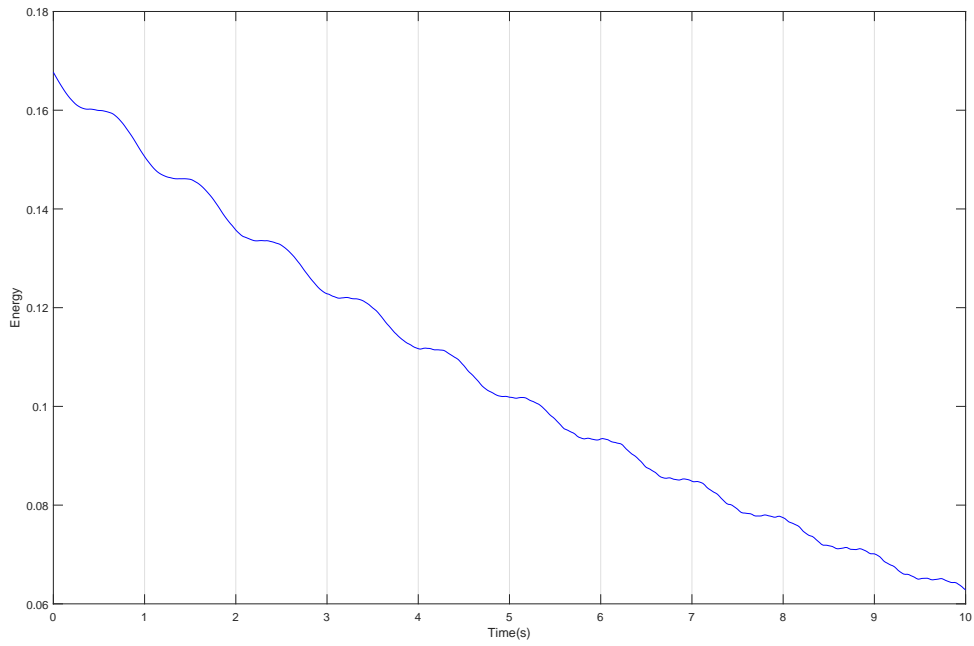


Figure 4: Decay of energy demonstrated with a 10x10 mesh grid and $k_1 = a_1 = a_2 = 0$, $k_0 = 0.1$ and $v(x, y; 0) = x$

We also demonstrate decay of the energy in the presence of some damping. In a similar case to the above, but taking a small amount of frictional damping $k_0 = 0.1$, we observe the energy decreasing. Figure 4 is produced by the script and demonstrates the dissipation of energy in the system.

6 Table of Variables

In the script that was generated in correspondence to this document, there are many variables that can be modified in order to fit the desired situation. Table 1 contains a list of the names and descriptions of each of these variables.

Variable	Description
D	Stiffness parameter for the cantilever material
Lx	Length of the cantilever in the x direction
Ly	Length of the cantilever in the y direction
Nx	Number of points in the mesh in the x direction
Ny	Number of points in the mesh in the y direction
N	Total number of node points where w is unknown
ν	Poisson Ratio
k_0	Linear damping parameter
k_1	Nonlinear damping parameter
a_1	Flow parameter in the x direction
a_2	flow parameter in the y direction
anim	Turns the animation on/off
energies	Turns the energy calculation on/off
t_0	Initial time of the calculation
t_f	Final time of the calculation
ns	Number of time steps taken

Table 1: Descriptions of each of the variables that can be chosen in the code

In addition to these variables, the user can also set the desired initial conditions using the functions described in Table 2.

Function	Description
winit(X, Y)	Sets the initial position of the cantilever. This is done by defining the internal variable wmat as a function of the X and Y positional arrays.
vinit(X, Y)	Sets the initial velocity of the cantilever. This is done by defining the internal variable vmat as a function of the X and Y positional arrays.

Table 2: Descriptions of each of the initial condition functions that can be chosen in the code

7 Acknowledgements

The author acknowledges the generous support of the National Science Foundation in this work through the grant entitled: “Collaborative Research: Experiment, Theory, and Simulation of Aeroelastic Limit Cycle Oscillations for Energy Harvesting Applications” (NSF-DMS 1908033).

A Matlab Code

```
1 close all;
2 %function specification here
3 %function [T,w,Le,Nle] = plate2dHH(tf,Lx,Ly,Nx,Ny,b1,b2,k0,k1,a1,a2,anim,
   energies)
4
5 %problem parameters
6 D = 1.0e-2; %stiffness parameter
7 Lx = 1; %length in x direction
8 Ly = 1; %length in y direction
9 Nx = 6; %number of nodes in x direction
10 Ny = 6; %number of nodes in y direction
11 N = (Nx-1)*(Ny); %total number of nodes where w is unknown
12 mu=0.3;
13 %b1 = 0.5;
14 %b2 = 1.0;
15 %k0 = 0.01; %damping parameter
16 %k1 = 0.01; %damping parameter
17 %a1 = 100;
18 %a2 = 0.5;
19 anim = 1; %see animation
20 energies = 0; %compute and plot energies
21
22 %timestepping parameters
23 t0 = 0; %initial time
24 tf = 10e0; %final time
25 ns = ceil(50*tf)+1; %number of time steps
26 t = linspace(t0, tf, ns); %time vector
27
28
29 %initialize spatial domain
30 x = linspace(0,Lx,Nx);
31 y = linspace(0,Ly,Ny);
32 [X,Y] = meshgrid(x,y);
33 dx = x(2)-x(1);
34 dy = y(2)-y(1);
35
36 %initialize solution array W = [wn; vn];
37 %get initial displacement and velocity - form W0
38 wn = winit(X,Y);
39 vn = vinit(X,Y);
40 W0 = [wn; vn]; %initial data vector is of length 2*N
41
42
43 % dydt = RHS(t,W0,D,Nx,Ny,N,x,y,dx,dy,mu);
44 % dydt = RHS(t,dydt,D,Nx,Ny,N,x,y,dx,dy,mu);
45 % dydt = RHS(t,dydt,D,Nx,Ny,N,x,y,dx,dy,mu);
46 % dydt = RHS(t,dydt,D,Nx,Ny,N,x,y,dx,dy,mu);
47
48 %call the timestepping code
49 tic;
50 [T,w] = ode15s(@(t,W) RHS(t,W,D,Nx,Ny,N,x,y,dx,dy,mu),t,W0);
51 odetime = toc;
52 fprintf('Total run time for ODE integrator: %g\n',odetime);
53
54 %postprocess the results
55 %plot the surface
56 wmat = [zeros(Ny,1) reshape(w(end,1:N),[Nx-1 Ny])'];
57
58 % figure(3); surf(X,Y,wmat); %plot the final surface
59 % xlabel({'w(x,y)'});
```

```

60 % ylabel({'y'});
61 % xlabel({'x'});
62 % title('Solution at final time');
63
64 %animate the solution
65 wvals=w(:,1:N);
66 wmax=max(max(abs(wvals)));
67 if anim>0
68     fig = figure(11);%hold on
69     F(ns) = struct('cdata',[],'colormap',[]);
70     grid on;
71     plt=surf(X,Y,[zeros(Ny,1) reshape(w(1,1:N),[Nx-1 Ny])' ]);
72     colormap(jet(256));
73     colorbar;
74     caxis([-1.1*wmax,1.1*wmax]);
75     zlim([-1.1*wmax,1.1*wmax])
76     view(-40,30);
77     str=sprintf('t = %3.3f',T(1));
78     h=text(0.95,0.95,0.9*wmax,str,'FontSize',12);
79     F(1) = getframe(fig);
80     for j = 2:ns
81         plt.ZData =[zeros(Ny,1) reshape(w(j,1:N),[Nx-1 Ny])'];
82         str=sprintf('t = %3.3f',T(j));
83         set(h,'String',str);
84         drawnow % display updates
85         F(j) = getframe(fig);
86     end
87     movie(fig,F,2,anim*ns/10);
88
89     vid = VideoWriter('animation.mp4','MPEG-4');
90     open(vid);
91     writeVideo(vid,F);
92     close(vid);
93 end
94
95 % compute energies if desired
96 if energies==1
97     tic;
98     %compute and plot energies
99     Le = zeros(size(ns));
100    Nle = zeros(size(ns));
101    for j=1:ns
102        [Le(j),Nle(j)] = computeEnergies(w(j,:),Nx,Ny,x,y,dx,dy,D,b1,b2);
103    end
104    energytime = toc;
105    fprintf('Total run time for energy calculation: %g\n',energytime);
106    figure;hold
107    plot(T,Le,'-b','DisplayName','E(t)');
108    plot(T,Nle,'-r','DisplayName','\tilde{E}(t)');
109    legend('linear E(t)','nonlinear E(t)')
110 end
111
112 %end
113
114
115
116 %function for initial displacement
117 function w = winit(X,Y)
118
119 Lx = X(1,end); %get Lx
120 Ly = Y(end,1); %get Ly
121 [Ny,Nx] = size(X); %get Nx and Ny

```

```

122 wmat = (-4*X.^5+15*X.^4-20*X.^3+10*X.^2); %define the initial value of w
123 %wmat = 0.0*X; %define the initial value of w
124 figure; surf(X,Y,wmat); %plot the initial surface
125 zlabel({'w(x,y)'});
126 ylabel({'y'});
127 xlabel({'x'});
128 title('Initial Displacement');
129 wmat = wmat(:,2:Nx); %trim off left values
130 w = reshape(wmat',[],1); %reshape matrix into the w vector
131 end
132
133 %function for initial velocity
134 function v = vinit(X,Y)
135 Lx = X(1,end); %get Lx
136 Ly = Y(end,1); %get Ly
137 [Ny,Nx] = size(X); %get Nx and Ny
138 vmat = 0.0*X* Lx * Ly; %define the initial value of w
139 % figure; surf(X,Y,vmat); %plot the initial surface
140 % % Create zlabel
141 % zlabel({'v(x,y)'});
142 % % Create ylabel
143 % ylabel({'y'});
144 % % Create xlabel
145 % xlabel({'x'});
146 % title('Initial Velocity');
147 vmat = vmat(:,2:Nx); %trim off left
148 v = reshape(vmat',[],1); %reshape matrix into the w vector
149 end
150
151 %function for computing energies
152 function [le,nle] = computeEnergies(w,Nx,Ny,x,y,dx,dy,D,b1,b2)
153 N = (Nx-2)*(Ny-2); %total number of nodes where w is unknown
154 %separate the displacements from velocities
155
156 %displacements in matrix form, include padded zeros on left and right
157 wmat = [zeros(1,Nx); [zeros(Ny-2,1) reshape(w(1:N),[Nx-2 Ny-2])] zeros(Ny
    -2,1)]; zeros(1,Nx)];
158 vmat = [zeros(1,Nx); [zeros(Ny-2,1) reshape(w(N+1:2*N),[Nx-2 Ny-2])] zeros(Ny
    -2,1)]; zeros(1,Nx)]; %velocities in matrix form
159
160 %compute the appropriate derivatives at the interior points
161 [laplacex,laplacey] = laplace(wmat,Nx,Ny,dx,dy);
162 %compute the integral of grad w squared
163 normlaplace2 = trapz(y,trapz(x,laplacex.*laplacex +laplacey.*laplacey,2));
164
165 %compute the integral of the velocities squared
166 normvel2 = trapz(y,trapz(x,vmat.*vmat,2));
167
168 %compute the appropriate derivatives at the interior points
169 [gradx,grady] = grads(wmat,Nx,Ny,dx,dy);
170
171 %compute the integral of grad w squared
172 normgrad2 = (trapz(y,trapz(x,gradx.*gradx + grady.*grady,2)));
173 normgrad4 = normgrad2^2;
174
175
176 %compute linear energy
177 le = 0.5*D*normlaplace2 + 0.5*normvel2 - (b1/2) * normgrad2;
178 nle= le - (b2/4) * normgrad4;
179
180 end
181 function [lx,ly] = laplace(w,Nx,Ny,dx,dy)

```

```

182
183 %initialize the output arrays
184 lx = zeros(size(w));
185 ly = zeros(size(w));
186 %apply BCs to wmat so we can compute w_xx and w_yy
187 %build the array with ghost nodes
188 w = [zeros(1,size(w,2)+2); [zeros(size(w,1),1), w, zeros(size(w,1),1)]; zeros
      (1,size(w,2)+2)];
189 %Applying hinged-hinged conditions
190 w(1,:) = -1.0 * w(3,:);
191 w(end,:) = -1.0 * w(end-2,:);
192
193 w(:,1) = -1.0 * w(:,3);
194 w(:,end) = -1.0 * w(:,end-2);
195
196 %loop over interior nodes and compute w_x and w_y using 2nd order centered
197 %differences
198 for j = 2:Nx+1 %which row of nodes
199     for i=2:Ny+1 %which column of nodes
200         lx(i-1,j-1) = (1/(dx^2))*(w(i,j+1)-2*w(i,j)+w(i,j-1)); %w_xx
          calculation
201         ly(i-1,j-1) = (1/(dy^2))*(w(i+1,j)-2*w(i,j)+w(i-1,j)); %w_yy
          calculation
202     end
203 end
204 end
205
206 function [gx,gy] = grads(w,Nx,Ny,dx,dy)
207
208 gx = zeros(size(w));
209 gy = zeros(size(w));
210
211 %apply BCs to wmat so we can compute w_xx and w_yy
212 %build the array with ghost nodes
213 w = [zeros(1,size(w,2)+2); [zeros(size(w,1),1), w, zeros(size(w,1),1)]; zeros
      (1,size(w,2)+2)];
214 %Applying hinged-hinged conditions
215 w(1,:) = -1.0 * w(3,:);
216 w(end,:) = -1.0 * w(end-2,:);
217
218 w(:,1) = -1.0 * w(:,3);
219 w(:,end) = -1.0 * w(:,end-2);
220 %loop over interior nodes and compute w_x and w_y using 2nd order centered
221 %differences
222 for j = 2:Ny+1 %which row of nodes
223     for i=2:Nx-1 %which column of nodes
224         gx(j-1,i) = (1/(2*dx))*(w(j,i+1)-w(j,i-1)); %w_x calculation
225         gy(j-1,i) = (1/(2*dy))*(w(j+1,i)-w(j-1,i)); %w_y calculation
226     end
227 end
228 end
229
230 %define the forcing function f(x,y,t)
231 function z = f(~,~,~)
232 z=0;
233 end
234
235 %define the ODE RHS function
236 function dydt=RHS(t,W,D,Nx,Ny,N,x,y,dx,dy,mu)
237 fprintf('Time: %g\n',t);
238 %reshape W into a matrix with 2*Ny rows and Nx-2 columns
239 wmat = reshape(W,[Nx-1 2*(Ny)]);

```

```

240 w = wmat(1:Ny,:); %displacements at interior nodes
241 v = wmat(Ny+1:2*Ny,:); %velocities at interior nodes
242
243 %initialize dydt
244 dydt = zeros(size([w;v]));
245 dydt(1:Ny,1:Nx-1) = v; %place v values in the w_t locations
246
247 %pad w matrix with edge conditions
248 w = [zeros(Ny,1) w];
249
250 %compute the RHS of the velocity equation
251
252 %solutions taken from MV Barton paper as is
253
254 %point adjacent to a fixed edge
255 for i = 3:Ny-2
256     j = 2;
257     dydt(Ny+i,j-1) = -D * (1/(dx^4))*(21 * w(i,j) - 8 * (w(i+1,j) + w(i,j+1) +
        w(i-1,j)) + 2*(w(i+1,j+1)+w(i-1,j+1)) + w(i+2,j) + w(i-2,j) + w(i,j+2));
258 end
259
260 %point adjacent to fixed free corner
261     %northwest
262     i = 2;
263     j = 2;
264     dydt(Ny+i,j-1) = -D * (1/(dx^4))*(20 * w(i,j) - 8 * (w(i+1,j) + w(i,j+1)) +
        (-6 + 2 * mu) * w(i-1,j) + 2*w(i+1,j+1) + (2 - mu) * w(i-1,j+1) + w(i+2,j)
        ) + w(i,j+2));
265
266     %southwest
267     i=Ny-1;
268     j=2;
269     dydt(Ny+i,j-1) = -D * (1/(dx^4))*(20 * w(i,j) - 8 * (w(i-1,j) + w(i,j+1)) +
        (-6 + 2 * mu) * w(i+1,j) + 2*w(i-1,j+1) + (2 - mu) * w(i+1,j+1) + w(i-2,j)
        ) + w(i,j+2));
270
271 %Point adjacent to fixed corner on free edge
272     %northwest corner
273     i = 1;
274     j = 2;
275     dydt(Ny+i,j-1) = -D * (1/(dx^4))*((17-8*mu-5*mu^2) * w(i,j) + (-12 + 4*mu) *
        w(i+1,j) + (-8 + 4*mu+4*mu^2)* w(i,j+1) + (4 + 2 * mu) * w(i+1,j+1) + 2 *
        w(i+2,j) + (1-mu^2) * w(i,j+2));
276
277     %southwest corner
278     i=Ny;
279     j=2;
280     dydt(Ny+i,j-1) = -D * (1/(dx^4))*((17-8*mu-5*mu^2) * w(i,j) + (-12 + 4*mu) *
        w(i-1,j) + (-8 + 4*mu+4*mu^2)* w(i,j+1) + (4 + 2 * mu) * w(i-1,j+1) + 2 *
        w(i-2,j) + (1-mu^2) * w(i,j+2));
281
282 %point on free edge
283     %north edge
284     for j = 3:Nx-2
285         i = 1;
286         dydt(Ny+i,j-1) = -D * (1/(dx^4))*((16-8*mu-6*mu^2) * w(i,j) + (-12 + 4*mu)
            * w(i+1,j) + (-8 + 4*mu+4*mu^2)* ( w(i,j-1) + w(i,j+1) ) + (4 + 2 * mu)
            * ( w(i+1,j+1) + w(i+1,j-1) ) + 2 * w(i+2,j) + (1-mu^2) * ( w(i,j-2) + w
            (i,j+2) ) );
287     end
288     %south edge
289     for j = 3:Nx-2

```

```

290     i = Ny;
291     dydt(Ny+i,j-1) = -D * (1/(dx^4))*((16-8*mu-6*mu^2) * w(i,j) + (-12 + 4*mu
) * w(i-1,j) + (-8 + 4*mu+4*mu^2)* ( w(i,j-1) + w(i,j+1) ) + (4 + 2 * mu)
    * ( w(i-1,j+1) + w(i-1,j-1) ) + 2 * w(i-2,j) + (1-mu^2) * ( w(i,j-2) + w
(i,j+2) ) );
292 end
293 %east edge
294 for i = 3:Ny-2
295     j = Nx;
296     dydt(Ny+i,j-1) = -D * (1/(dx^4))*((16-8*mu-6*mu^2) * w(i,j) + (-12 + 4*mu
) * w(i,j-1) + (-8 + 4*mu+4*mu^2)* ( w(i-1,j) + w(i+1,j) ) + (4 + 2 * mu)
    * ( w(i+1,j-1) + w(i-1,j-1) ) + 2 * w(i,j-2) + (1-mu^2) * ( w(i-2,j) + w
(i+2,j) ) );
297 end
298
299 %Point adjacent to free edge
300 %north edge
301 for j = 3:Nx-2
302     i = 2;
303     dydt(Ny+i,j-1) = -D * ( 19 * w(i,j) + -8 * ( w(i+1,j) + w(i,j-1) + w(i,j
+1) ) + (-6 + 2*mu) * w(i-1,j) + 2 * (w(i+1,j+1) + w(i+1,j-1)) + (2 - mu)
    * (w(i-1,j+1) + w(i-1,j-1)) + w(i+2,j) + w(i,j-2) + w(i,j+2) );
304 end
305 %south edge
306 for j = 3:Nx-2
307     i = Ny-1;
308     dydt(Ny+i,j-1) = -D * (1/(dx^4))* ( 19 * w(i,j) + -8 * ( w(i-1,j) + w(i,j
-1) + w(i,j+1) ) + (-6 + 2*mu) * w(i+1,j) + 2 * (w(i-1,j+1) + w(i-1,j-1))
    + (2 - mu) * (w(i+1,j+1) + w(i+1,j-1)) + w(i-2,j) + w(i,j-2) + w(i,j+2)
);
309 end
310 %east edge
311 for i = 3:Ny-2
312     j = Nx-1;
313     dydt(Ny+i,j-1) = -D * (1/(dx^4))* ( 19 * w(i,j) + -8 * ( w(i+1,j) + w(i,j
-1) + w(i-1,j) ) + (-6 + 2*mu) * w(i,j+1) + 2 * (w(i-1,j-1) + w(i+1,j-1))
    + (2 - mu) * (w(i-1,j+1) + w(i-1,j+1)) + w(i+2,j) + w(i,j-2) + w(i-2,j)
);
314 end
315
316 %Point on free corner
317 %northeast
318 i = 1;
319 j = Nx;
320 dydt(Ny+i,j-1) = -D * (1/(dx^4))* ( (12-8*mu - 4*mu^2) * w(i,j) + (-12 + 8*mu
+ 4*mu^2) * ( w(i+1,j) + w(i,j-1) ) + (8 - 8*mu) * w(i+1,j-1) + (2 - 2*mu
^2) * (w(i+2,j) + w(i,j-2)) );
321
322 %southeast
323 i = Ny;
324 j = Nx;
325 dydt(Ny+i,j-1) = -D * (1/(dx^4))* ( (12-8*mu - 4*mu^2) * w(i,j) + (-12 + 8*mu
+ 4*mu^2) * ( w(i-1,j) + w(i,j-1) ) + (8 - 8*mu) * w(i-1,j-1) + (2 - 2*mu
^2) * (w(i-2,j) + w(i,j-2)) );
326
327 %Points inside free free corner
328 %northeast
329 i = 2;
330 j = Nx-1;
331 dydt(Ny+i,j-1) = -D * (1/(dx^4))* ( 18 * w(i,j) + -8 * ( w(i+1,j) + w(i,j-1)
) + (-6 + 2*mu) * ( w(i,j+1) + w(i-1,j) ) + (2 - mu) * (w(i+1,j+1) + w(i
-1,j-1)) + 2 * w(i+1,j-1) + (2 - 2*mu^2) * w(i-1,j+1) + w(i+2,j) + w(i,j

```



```

-2));
332
333 %southeast
334 i = Ny-1;
335 j = Nx-1;
336 dydt(Ny+i,j-1) = -D * (1/(dx^4))*( 18 * w(i,j) + -8 * ( w(i-1,j) + w(i,j-1))
+ (-6 + 2*mu) * ( w(i,j+1) + w(i+1,j) ) + (2 - mu) * (w(i-1,j+1) + w(i
+1,j-1)) + 2 * w(i-1,j-1) + (2 - 2*mu^2) * w(i+1,j+1) + w(i-2,j) + w(i,j
-2));
337
338 %Poitns adjacent to free free corner on free edge
339 %north - east edge
340 i = 2;
341 j = Nx;
342 dydt(Ny+i,j-1) = -D * (1/(dx^4))*( (15-8*mu - 4*mu^2) * w(i,j) + (-8 + 4*mu +
4*mu^2) * w(i+1,j) + (-6 + 4*mu + 2*mu^2) * w(i-1,j) + (-12 + 4*mu) * w(
i,j-1) + (4 - 2*mu) * (w(i+1,j-1) + w(i-1,j-1)) + (1-mu^2) * w(i+2,j) + 2
* w(i,j-2) );
343 %south - east edge
344 i = Ny-1;
345 j = Nx;
346 dydt(Ny+i,j-1) = -D * (1/(dx^4))*( (15-8*mu - 4*mu^2) * w(i,j) + (-8 + 4*mu +
4*mu^2) * w(i-1,j) + (-6 + 4*mu + 2*mu^2) * w(i+1,j) + (-12 + 4*mu) * w(
i,j-1) + (4 - 2*mu) * (w(i-1,j-1) + w(i+1,j-1)) + (1-mu^2) * w(i-2,j) + 2
* w(i,j-2) );
347
348 %north edge
349 i = 1;
350 j = Nx-1;
351 dydt(Ny+i,j-1) = -D * (1/(dx^4))*( (15-8*mu - 4*mu^2) * w(i,j) + (-8 + 4*mu +
4*mu^2) * w(i,j-1) + (-6 + 4*mu + 2*mu^2) * w(i,j+1) + (-12 + 4*mu) * w(
i+1,j) + (4 - 2*mu) * (w(i+1,j+1) + w(i+1,j-1)) + (1-mu^2) * w(i,j-2) + 2
* w(i+2,j) );
352
353 %south edge
354 i = Ny;
355 j = Nx-1;
356 dydt(Ny+i,j-1) = -D * (1/(dx^4))*( (15-8*mu - 4*mu^2) * w(i,j) + (-8 + 4*mu +
4*mu^2) * w(i,j-1) + (-6 + 4*mu + 2*mu^2) * w(i,j+1) + (-12 + 4*mu) * w(
i-1,j) + (4 - 2*mu) * (w(i-1,j+1) + w(i-1,j-1)) + (1-mu^2) * w(i,j-2) + 2
* w(i-2,j) );
357
358 %interior points
359 for i=3:Ny-2
360 for j=3:Nx-2
361 dydt(Ny+i,j-1) = -D * (1/(dx^4))*(20 * w(i,j) - 8 * (w(i+1,j) + w(i,j
+1) + w(i-1,j) + w(i,j-1) ) + 2*(w(i+1,j+1)+w(i-1,j+1)+w(i+1,j-1)+w(i-1,j
-1)) + w(i+2,j) + w(i-2,j) + w(i,j+2) + w(i,j-2));
362 end
363 end
364
365 dydt = reshape(dydt',[2*N 1]);
366
367 end

```

References

- [1] Dieter Bahlmann and Ulrich Langer. “A fast solver for the first biharmonic boundary value problem”. In: *Numerische Mathematik* 63.1 (1992), pp. 297–313.
- [2] MV Barton. *Finite difference equations for the analysis of thin rectangular plates with combinations of fixed and free edges*. Tech. rep. TEXAS UNIV AT AUSTIN DEFENSE RESEARCH LAB, 1948.
- [3] Heribert Blum, Rolf Rannacher, and Rolf Leis. “On the boundary value problem of the biharmonic operator on domains with angular corners”. In: *Mathematical Methods in the Applied Sciences* 2.4 (1980), pp. 556–581.
- [4] Fioralba Cakoni, George C Hsiao, and Wolfgang L Wendland. “On the boundary integral equation method for a mixed boundary value problem of the biharmonic equation”. In: *Complex Variables, Theory and Application: An International Journal* 50.7-11 (2005), pp. 681–696.
- [5] Maria Deliyianni and Justin T Webster. “Theory of Solutions for An Inextensible Cantilever”. In: *Applied Mathematics & Optimization* (2021), pp. 1–55.
- [6] Maria Deliyianni et al. “Dynamic equations of motion for inextensible beams and plates”. In: *arXiv preprint arXiv:2107.07454* (2021).
- [7] Maria Deliyianni et al. “Large deflections of inextensible cantilevers: modeling, theory, and simulation”. In: *Mathematical Modelling of Natural Phenomena* 15 (2020), p. 44.
- [8] Earl Dowell and Kevin McHugh. “Equations of motion for an inextensible beam undergoing large deflections”. In: *Journal of Applied Mechanics* 83.5 (2016), p. 051007.
- [9] Louis W Ehrlich. “Solving the biharmonic equation as coupled finite difference equations”. In: *SIAM Journal on Numerical Analysis* 8.2 (1971), pp. 278–287.
- [10] Jason Howell et al. “A thorough look at the (in) stability of piston-theoretic beams”. In: *arXiv preprint arXiv:1903.07244* (2019).
- [11] Jason S Howell, Daniel Toundykov, and Justin T Webster. “A cantilevered extensible beam in axial flow: semigroup well-posedness and postflutter regimes”. In: *SIAM Journal on Mathematical Analysis* 50.2 (2018), pp. 2048–2085.
- [12] PCM Lau. “Curvilinear finite difference method for biharmonic equation”. In: *International Journal for Numerical Methods in Engineering* 14.6 (1979), pp. 791–812.
- [13] DM Tang and EH Dowell. “Aeroelastic response and energy harvesting from a cantilevered piezoelectric laminated plate”. In: *Journal of Fluids and Structures* 76 (2018), pp. 14–36.
- [14] DM Tang, Dani Levin, and EH Dowell. “Experimental and theoretical correlations for energy harvesting from a large flapping flag response”. In: *Journal of Fluids and structures* 86 (2019), pp. 290–315.